Bifurcations of Monodromic Heteroclinic Contours in Planar Systems

Introduction to Nonlinear Dynamical Systems - Project

Pedro Basto da Silva - 8258996

February 10, 2025

Abstract

Smooth planar vector fields containing two hyperbolic saddles may possess contours formed by heteroclinic connections between said saddles. We start by introducing some basic notions that will be helpful in following and understanding the rest of the work. We then present an overview of known derivations and results on bifurcations of monodromic heteroclinic contours for two different subcases, related to different properties of saddle eigenvalues. At the end, we give a two-dimensional polynomial system containing such a contour, which is then studied under a two-parameter perturbation. It is shown that the numerical analysis corroborates the theoretically predicted phenomena, including a variety of homo- and heteroclinic connections.

1 Introduction

Heteroclinic contours are critical structures in planar dynamical systems, arising naturally in the study of vector fields. These contours are formed by two trajectories connecting two saddle-type equilibria, often enclosing a region where the system exhibits different behavior, such as periodic orbits or other recurring dynamics. These configurations of saddles and orbits are alternatively called *polygon* and *polycycle* [1]. The nature of these contours and their stability can change significantly under the variation of system parameters, leading to bifurcations that alter the qualitative behavior of the vector field at some critical parameter values.

Planar heteroclinic contours can be subdivided into two categories, namely monodromic and non-monodromic. There are already detailed theoretical studies for both cases, such as the ones published in [1], [2] and [3]. In both cases, depending on the eigenvalues of the saddles, either one limit cycle or two limit cycles of opposite stability are generated as the result of homoclinic bifurcations.

The aim of this report is to explore specifically the bifurcations of monodromic heteroclinic contours in planar systems, presenting a detailed analysis of existing results and their derivations. This study focuses on constructing a bifurcation diagram that maps the transitions of a system's dynamics as the parameters are varied. For this purpose, some basic notions are first introduced before diving into concrete derivations.

To illustrate these theoretical findings, an explicit example of a polynomial system is given, which can be perturbed to bifurcate as predicted in the theoretical part, allowing for a direct comparison between the analytical predictions and numerical or qualitative observations. This approach not only clarifies the underlying mechanisms driving bifurcations but also highlights the practical implications of these phenomena in the broader context of planar dynamical systems.

2 Base Notions

2.1 Planar Vector Fields

Let $X := (x\ y)^T$ be a point in the plane $\mathbb{R}^2$. A general planar system can be written as

$$\dot{X} = F(X) \equiv \begin{pmatrix} P(x,y) \\ Q(x,y) \end{pmatrix}, \tag{1}$$

where P and Q are smooth $\mathbb{R}^2 \to \mathbb{R}$ functions. The map $(x, y) \mapsto (P(x, y), Q(x, y))$ is called a smooth vector field, defining, for small values of $t \in \mathbb{R}$, a local flow $\varphi^t : \mathbb{R}^2 \mapsto \mathbb{R}^2$. We can then write $X(t) = \varphi^t(X_0)$ as the unique solution of the system (1), satisfying the initial condition $X(0) = X_0$.

If we denote I as the maximal definition interval of a solution $t \mapsto X(t)$ with $t \in I$, then the image oriented by the advance of time $X(I) \subset \mathbb{R}^2$ is called the orbit starting at X_0, and is denoted by $\Gamma(X_0)$. Additionally, the orbit containing X^0 is defined as

$$\{\varphi\left(X^0, t\right) \mid t \in I\left(X^0\right)\} \subset \mathbb{R}^2. \tag{2}$$

The above definition, along with the appropriate orientation, makes up $\Gamma(X_0)$. We can naturally define the forward and backward orbits corresponding to $t \geq 0$ and $t \leq 0$, respectively. By drawing a collection of orbits in the $\mathbb{R}^2$ plane along with the direction of the vector field, we get the phase portrait, which helps to determine the behavior of the system. To describe the flow starting at a certain point, we can more generally define a solution curve as $\gamma(t) = \varphi(X^0, t)$.

2.2 Equilibria

Given a system (1), a point $X^0 = (x^0, y^0)$ satisfying

$$P\left(x^0, y^0\right) = Q\left(x^0, y^0\right) = 0 \tag{3}$$

is called an equilibrium, for which the Jacobian matrix allows us to classify them. An equilibrium X^0 is hyperbolic if $\mathrm{Re}(\lambda_{1,2}) \neq 0$, and within this category we can distinguish foci, if both eigenvalues are complex, nodes, if both eigenvalues are real with equal sign, and saddles, where both eigenvalues are real and of opposing signs. For a general vector field we may compute the respective Jacobian matrix, which defines a linear approximation at a given point.

Theorem 2.1 *(Grobman-Hartman) Consider a vector field containing a hyperbolic equilibrium X^0. Then, this equilibrium has a neighborhood, in which the phase portrait is homeomorphic to that of the locally linearized system .*

In consequence, for hyperbolic equilibria, we can distinguish different cases based on the eigenvalues of the Jacobian matrix, commonly referred to as the eigenvalues of the fixed point itself. In the case of a saddle point, which will be of the most importance in this work, the pair of real eigenvalues of opposing sign are denoted by $\lambda_s < 0 < \lambda_u$. Along the eigenvectors associated with these values, solutions in a phase portrait either move directly towards the saddle (for λ_s) or away from it (for λ_u), hence the notation s for stable and u for unstable. Thus, saddles have associated with them two orbits converging to it when $t \to \infty$ and two other orbits diverging at the same time.

In a general setting, the role of the eigenvectors is played by the stable and unstable manifolds of X^0, which are the sets

$$\begin{aligned} W^s\left(X^0\right) &:= \{X \in \mathbb{R}^2 : \varphi^t(X) \to X^0 \ \text{ as } t \to \infty\} \\ W^u\left(X^0\right) &:= \{X \in \mathbb{R}^2 : \varphi^t(X) \to X^0 \ \text{ as } t \to -\infty\}, \end{aligned} \tag{4}$$

where both manifolds of X^0 consist of two separatrices.

2.3 Cycles and Poincaré Map

Consider a solution $\gamma(t)$ of system (1) for which there exists a minimal interval $T > 0$ such that $\gamma(t + T) = \gamma(t)$ for all $t \in \mathbb{R}$. This solution is said to be periodic with period T, and its orbit is referred to as a cycle.

Let X_0 be a point in the cycle; since the vector field containing this cycle is smooth, we can introduce a cross section Σ at X_0, which is a line segment orthogonal to the cycle. In this cross section, we may define a smooth coordinate ξ, where the point $\xi = 0$ coincides with X_0. Note that the periodic solution through X_0 returns to Σ after time T. By smoothness, solutions starting at a point $X \in \Sigma$ close to X_0 also return to Σ close to X_0 after completing a trajectory near the cycle.

Thus, we obtain a discrete and locally defined smooth map $P : \Sigma \to \Sigma$ called the Poincaré map associated with the cycle. The cycle at $\xi = 0$ is a fixed point of the Poincaré map yielding $P(0) = 0$. In fact, any fixed point of the Poincaré map corresponds to a cycle.

2.4 Connections

In linear vector fields, the stable and unstable manifolds of an equilibrium intersect only at the saddle itself, and Theorem 2.1 asserts that nonlinear systems are locally the same. However, globally the system can behave differently. It may be the case that an orbit approaching X^0 coincides with an orbit leaving X^0. Therefore, there exists a solution γ such that

$$\lim_{t\to-\infty} \gamma(t) = \lim_{t\to\infty} \gamma(t) = X^0. \tag{5}$$

The orbit associated with these solutions is known as a homoclinic connection. Depending on the position of the other separatrices, a homoclinic orbit can be either samll or big, as seen in Figure 1.

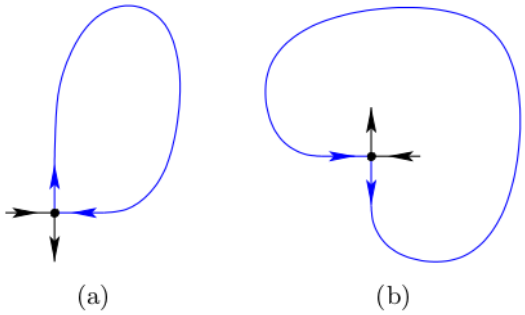

Figure 1: Homoclinic connections to saddles: small (a) and big (b). Image taken from [4].

In addition to solutions that connect a saddle point to itself, we may also find solutions that connect two different saddle points. Consider a vector field with two saddles X^0 and X^1, then there may exist γ such that

$$\lim_{t\to-\infty} \gamma(t) = X^0 \text{ and } \lim_{t\to\infty} \gamma(t) = X^1. \tag{6}$$

The orbit associated with such a case is called a heteroclinic connection, which can be seen in Figure 2.

Figure 2: Heteroclinic connection between two saddles. Image taken from [4].

In order to study phase portraits with these types of homoclinic and heteroclinic connections, there are some important quantities that need to be defined. The saddle quantity of X^0, $\sigma = \lambda_s + \lambda_u = (div\ F)(X^0)$ (which is a real number), and the saddle index $\lambda = -\lambda_s/\lambda_u$ (which is a positive real number) are values that will be helpful later when trying to distinguish various scenarios. Saddles with $\lambda > 1$ are called dissipative, while saddles with $\lambda < 1$ are called non-dissipative.

3 Heteroclinic Contours

In special planar systems, for example, with invariant coordinate axes, two saddles on that axis can be connected by one heteroclinic orbit. However, if another heteroclinic connection occurs between the same fixed points, a heteroclinic contour is formed. Consider a planar vector field as in system (1) and assume that it has two hyperbolic equilibria of saddle type, which we label L and M. Let $\lambda_s < 0 < \lambda_u$ and $\mu_s < 0 < \mu_u$ be the eigenvalues of L and M, respectively, with corresponding saddle indices

$$\lambda = -\frac{\lambda_s}{\lambda_u},\ \mu = -\frac{\mu_s}{\mu_u}. \tag{7}$$

Suppose also that this system has solutions $\gamma_1(t)$ and $\gamma_2(t)$ satisfying

$$\begin{aligned} \lim_{t\to-\infty} \gamma_1(t) = L \text{ and } \lim_{t\to\infty} \gamma_1(t) = M, \\ \lim_{t\to-\infty} \gamma_2(t) = M \text{ and } \lim_{t\to\infty} \gamma_2(t) = L. \end{aligned} \tag{8}$$

We see that the orbits of $\gamma_1(t)$ and $\gamma_2(t)$ are heteroclinic connections between L and M in opposite directions. Together with the saddles, they form the previously mentioned heteroclinic contour. Depending on the position of the stable and unstable manifolds of L and M, there are two distinct possible types of heteroclinic contours called monodromic and nonmonodromic, as seen in Figure 3.

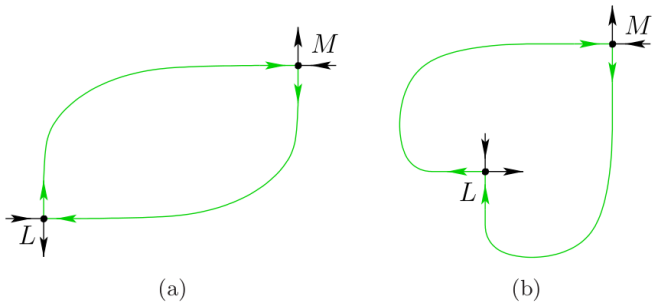

Figure 3: The two types of heteroclinic contours. (a) Monodromic and (b) nonmonodromic. Both images taken from [5].

To understand this choice of terminology, note that the monodromic contour may be approached as a limit set by solutions inside the contour. It is also possible to contain all stable and unstable manifolds inside the contour, in which case the contour may be approached as a limit set for solutions outside the contour. This case is also monodromic, but is topologically equivalent to the depicted one, and thus will not be considered.

We will see that the bifurcation diagrams in both cases strongly depend on the values of λ, μ and also $\lambda\mu$. Especially, it is important whether these quantities are smaller or larger than 1. Recall that saddles with index greater than one are called dissipative. In principle, the generic subcases given in Table (1) are possible.

1	$\lambda < 1$	$\mu > 1$	$\lambda\mu < 1$
2	$\lambda < 1$	$\mu > 1$	$\lambda\mu > 1$
3	$\lambda > 1$	$\mu < 1$	$\lambda\mu > 1$
4	$\lambda > 1$	$\mu < 1$	$\lambda\mu < 1$
5	$\lambda > 1$	$\mu > 1$	$\lambda\mu > 1$
6	$\lambda < 1$	$\mu < 1$	$\lambda\mu < 1$

Table 1: All possibilities for saddle indexes λ, μ and their product, regarding saddle points L and M, respectively. There is no specific reason for the ordering.

By reversing time and interchanging the roles of L and M, we notice that there are 2 to 4 essentially different subcases to consider. More specifically, reversing time, we see that 1 goes to 3 and 5 to 6. When changing the roles of L and M, 1 goes to 4 and 2 to 3. So, if we study only subcases 1 and 6, the results for all other subcases follow immediately. To conclude, in the following sections we consider only subcases $\lambda < 1$, $\mu < 1$ and $\lambda < 1$, $\mu > 1$, where $\lambda\mu < 1$ in both scenarios.

4 Bifurcations

Having defined the necessary objects which might appear in a phase portrait, we come to the concept of bifurcation. Consider a system

$$\begin{cases} \dot{x} = P(x, y, \alpha) \\ \dot{y} = Q(x, y, \alpha), \end{cases} \tag{9}$$

where $\alpha \in \mathbb{R}^n$ is an n-dimensional parameter. With the introduction of this parameter, the system (9) defines an n-dimensional family of vector fields. Variation of the parameter results in different vector fields, which in turn yield different phase portraits. However, we consider phase portraits to be equivalent whenever there exists a homeomorphism between them that preserves orbits, that is, takes orbits from one phase portrait to orbits of the other. If this is the case, we call the associated vector fields orbitally topologically equivalent.

A vector field is said to be structurally stable if there exists a neighborhood of it in the space of all smooth vector fields such that all vector fields from this neighborhood are orbitally topologically equivalent. For parameter-dependent systems this implies that if a system for a given value of α is structurally stable, then there exists a neighborhood of α in the parameter space such that for all parameter values in this neighborhood the corresponding systems are orbitally topologically equivalent.

A bifurcation is then a qualitative change of the phase portrait under variation of the parameter that results in a phase portrait that is not topologically equivalent to the original phase portrait, prior to chaning the parameter. An overview of the bifurcational behaviour of a family of vector fields can be given in the form of a bifurcation diagram. Such a diagram consists of a depiction of the parameter space which is partitioned into sets corresponding to orbitally topologically equivalent vector fields. From this sketch one can see at a glance for which values of the parameters which bifurcation occurs. The diagram is completed when, for all of these partitioning sets, a representative phase portrait is supplied.

5 Bifurcation of Heteroclinic Contours

We are now ready to describe bifurcations of planar monodromic heteroclinic contours in a generic two-parameter system. In this case, the bifurcation diagram corresponds to a sketch of the parameter-plane. Consider a smooth vector field as in the system (9) where P and Q are smooth functions of $\mathbb{R} \times \mathbb{R} \times \mathbb{R}^2$ to $\mathbb{R}$. We assume that for $\alpha = (0, 0)$ the system has a monodromic heteroclinic contour described in Section 3.

In a neighborhood of L for this specific system where $\alpha = (0, 0)$, we introduce two cross sections, Σ_L and Π_L, on the incoming and outgoing heteroclinic connections, respectively. In these cross sections, we introduce the coordinates ξ_L and η_L, respectively. We define these coordinates such that the points $\xi_L = 0$ and $\eta_L = 0$ coincide with the intersection of the stable and unstable manifolds and the respective cross sections and so that the positive values of the coordinates are inside the heteroclinic contour. Analogously, in a neighborhood of M, we introduce the cross sections Σ_M and Π_M furnished with the coordinates ξ_M and η_M with analogous properties. This can be seen in Figure 4.

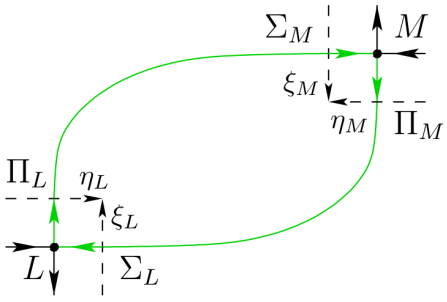

Figure 4: The monodromic contour with all cross sections and coordinates. Image taken from [5].

Using the cross sections, we define the splitting parameters β_1 and β_2 that measure the splitting of the heteroclinic connection along Σ_L and Σ_M, respectively. We can now define exact singular maps $\Delta_L : \Sigma_L \to \Pi_L$ and $\Delta_M : \Sigma_L \to \Pi_M$ by

$$\Delta_L(\xi_L) = \xi_L^{\lambda} \quad \text{and} \quad \Delta_M(\xi_M) = \xi_M^{\mu} \tag{10}$$

near the saddles, and truncated regular maps $Q : \Pi_L \to \Sigma_M$ and $R : \Pi_m \to \Sigma_L$ by

$$Q(\eta_L) = \beta_2 + \theta_1 \eta_L \quad \text{and} \quad R(\eta_M) = \beta_1 + \theta_2 \eta_M \tag{11}$$

near the heteroclinic connections where θ_1 and θ_2 are positive constants. No higher order terms are used in the singular and regular maps since it was shown by Reyn [1] that they do not change the topology of the bifurcation diagrams in both subcases. By composing these maps we arrive at the truncated Poincaré map $P : \Sigma_L \to \Sigma_L$ which becomes

$$\begin{aligned} P(\xi_L) &= (R \circ \Delta_M \circ Q \circ \Delta_L)(\xi_L) \\ &= \beta_1 + \theta_2 \left(\beta_2 + \theta_1 \xi_L^{\lambda}\right)^{\mu} . \end{aligned} \tag{12}$$

We now study the emergence of homoclinic connections. From the geometry of the monodromic contour, see Figure 5, it is seen that a homoclinic connection at L may only arise whenever $\beta_1 < 0$ and $\beta_2 > 0$.

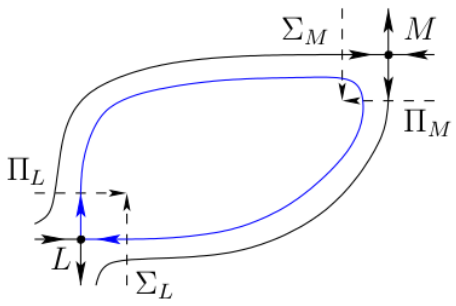

Figure 5: The appearance of a homoclinic connection at L. Image taken from [4].

Moreover, a homoclinic connection at L coincides with a solution of the equation

$$(R \circ \Delta_M \circ Q)(0) = \beta_1 + \theta_2 \beta_2^{\mu} = 0 \tag{13}$$

which can be rewritten into the expression

$$\beta_2 = \left(-\frac{\beta_1}{\theta_2}\right)^{\frac{1}{\mu}} . \tag{14}$$

A similar discussion can be had for the appearance of homoclinic connections at M. Firstly, such connections can only arise whenever $\beta_1 > 0$ and $\beta_2 < 0$. At M, a homoclinic connection coincides with a solution of the equation

$$(Q \circ \Delta_L \circ R)(0) = \beta_2 + \theta_1 \beta_1^{\lambda} = 0 \tag{15}$$

which we can rewrite into the expression

$$\beta_2 = -\theta_1 \beta_1^{\lambda} . \tag{16}$$

Thus, we find that there are two curves in the parameter-plane corresponding to homoclinic connections at L and M. We label these curves P_L and P_M, respectively. Sketching these curves in the parameter-plane is the first step towards the bifurcation diagram of heteroclinic contours. Depending on the two different subcases discussed at the end of Section 3, we obtain different curves, seen in Figure 6. For ease of reference, we label the two sectors of the parameter-plane delineated by P_L and P_M as A and B.

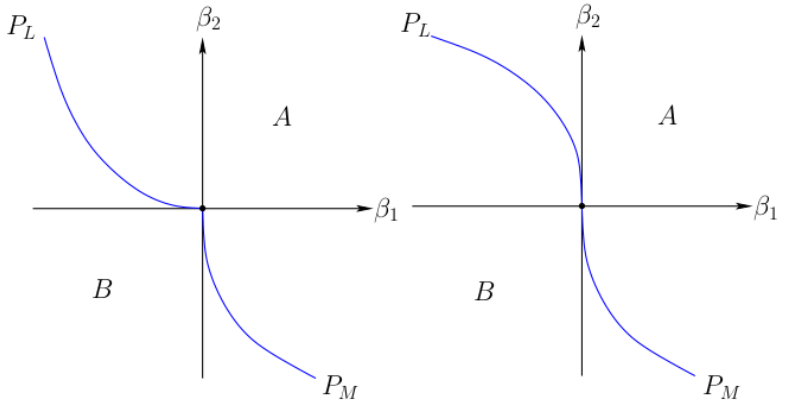

(a) $\lambda < 1$ and $\mu < 1$ (b) $\lambda < 1$ and $\mu > 1$

Figure 6: The emergence of homoclinic connections in the parameter-plane. Image taken from [4].

Now we can move on to limit cycles. As seen in Section 2.3, these correspond to fixed points of the Poincaré map (12). Therefore we look for solutions ξ_L of

$$\beta_1 + \theta_2 \left(\beta_2 + \theta_1 \xi_L^\lambda\right)^\mu = \xi_L \ . \tag{17}$$

This equation may be rewritten as

$$\beta_2 + \theta_1 \xi_L^\lambda = \left(\frac{\xi_L - \beta_1}{\theta_2}\right)^{\frac{1}{\mu}} \ . \tag{18}$$

To look for solutions of this equation we consider the left- and right-hand side separately. To this end, we define functions f and g by

$$f\left(\xi_L\right) = \beta_2 + \theta_1 \xi_L^\lambda \ \text{ and } \ g\left(\xi_L\right) = \left(\frac{\xi_L - \beta_1}{\theta_2}\right)^{\frac{1}{\mu}} \tag{19}$$

which allows us to rewrite Equation (18) as $f\left(\xi_L\right) = g\left(\xi_L\right)$. To study solutions of this equation, we will also need the derivatives of f and g which we find to be

$$f'\left(\xi_L\right) = \lambda \theta_1 \xi_L^{\lambda - 1} \ \text{ and } \ g'\left(\xi_L\right) = \frac{1}{\mu \theta_2} \left(\frac{\xi_L - \beta_1}{\theta_2}\right)^{\frac{1}{\mu} - 1} \ . \tag{20}$$

Additionally, the maps f and g have an intuitive geometric interpretation which will relate them to the generation of homoclinic connections. In terms of the model maps, we can see that $f = Q \circ \Delta_L$ while $g = \left(R \circ \Delta_M\right)^{-1}$. Thus, both can be seen as maps from Σ_L to Σ_M. This point of view makes it clear that the solution $f\left(0\right) = g\left(0\right)$ coincides with a homoclinic connection at L, while a solution $\xi_L > 0$ satisfying $f\left(\xi_L\right) = g\left(\xi_L\right) = 0$ coincides with a periodic orbit.

Furthermore, we have expressions for

$$f(0) = \beta_2 \ \text{ and } \ g(0) = \left(-\frac{\beta_1}{\theta_2}\right)^{\frac{1}{\mu}} \tag{21}$$

and we can find solutions to $f\left(\xi_L^f\right) = 0$ and $g\left(\xi_L^g\right) = 0$, namely,

$$\xi_L^f = \left(-\frac{\beta_2}{\theta_1}\right)^{\frac{1}{\lambda}} \ \text{ and } \ \xi_L^g = \beta_1 \ . \tag{22}$$

From this point forward, we have to treat both subcases separately.

5.1 The first subcase $\lambda < 1$, $\mu < 1$

As both λ, $\mu < 1$, the maps f and g have the limiting properties

$$\lim_{\xi_L \to 0} f(\xi_L) = \beta_2 \quad \text{and} \quad \lim_{\xi_L \to 0} f'(\xi_L) = \infty \tag{23}$$

while

$$\lim_{\xi_L \to \beta_1} g(\xi_L) = 0 \quad \text{and} \quad \lim_{\xi_L \to \beta_1} g'(\xi_L) = 0, \tag{24}$$

which tells us that f is convex upward while g is convex downward.

A useful observation is that in this case, for arbitrarily small parameters values, there are no small values of ξ_L where f and g have equal derivative. To see this, suppose that $f'(\xi_L) = g'(\xi_L)$ so that

$$\beta_1 = \xi_L - \theta_2 (\lambda\mu\theta_1\theta_2)^{\frac{\mu}{1-\mu}} \xi_L^{\frac{\mu(\lambda-1)}{1-\mu}} . \tag{25}$$

Noting that $\frac{\mu(\lambda-1)}{1-\mu} < 0$ given the restriction on λ and μ, we see that $\lim_{\xi_L \to 0} \beta_1(\xi_L) = -\infty$. Thus, letting ξ_L and the parameters go to zero, f and g cannot have the same derivative at ξ_L. This result locally excludes the tangency of f and g and also implies that there may be at most one intersection of f and g. As, by Rolle's theorem, between any two intersections of f and g we can find a point where they have equal derivative.

Suppose that we choose a pair (β_1, β_2) of parameters from sector A. For $\beta_1 < 0$ the point lies above P_L and for $\beta_1 > 0$ the point lies above P_M. Suppose $\beta_1 < 0$, we then have the following.

$$\beta_2 > \left(-\frac{\beta_1}{\theta_2}\right)^{\frac{1}{\mu}} \quad \text{so} \quad f(0) > g(0) \tag{26}$$

and $\beta_2 > 0$. This, together with their limiting properties, implies that f and g do not intersect for arbitrarily small values of β_1 and β_2, as can be seen in Figure 7(a).

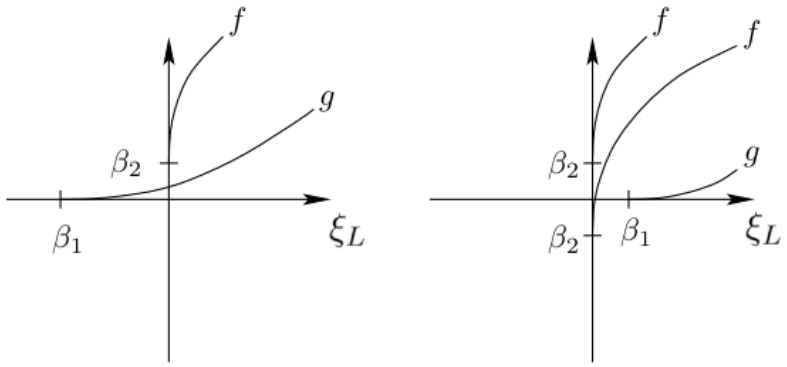

(a) $\beta_1 < 0$ (b) $\beta_1 > 0$

Figure 7: Possible configurations of f and g for parameters from sector A, when $\lambda, \mu < 1$. The coordinate x corresponds to ξ_L. Images adapted from [4].

In the case where $\beta_1 > 0$, we find that

$$\left(-\frac{\beta_2}{\theta_1}\right)^{\frac{1}{\lambda}} < \beta_1 \quad \text{so} \quad \xi_L^f < \xi_L^g \tag{27}$$

and $\beta_2 < 0$ or $\beta_2 > 0$. This again implies that f and g do not intersect for arbitrarily small values of β_1 and β_2, as seen in Figure 7(b). This leads to the conclusion that there are no limit cycles in sector A.

Moving on to sector B, we have for $\beta_1 < 0$ that we are below P_L, and for $\beta_1 > 0$ we are below P_M. Suppose then that $\beta_1 < 0$. Then we have $f(0) < g(0)$, while $\beta_2 < 0$ or $\beta_2 > 0$. In this case, we find that f and g intersect for arbitrarily small values of β_1 and β_2, as seen in Figure 8(a).

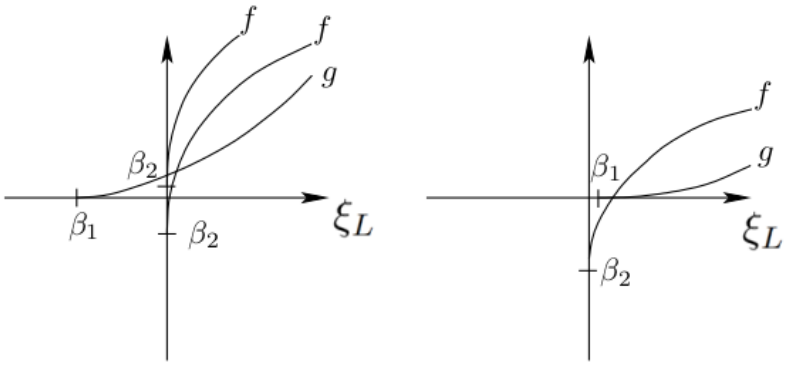

(a) $\beta_1 < 0$ (b) $\beta_1 > 0$

Figure 8: Possible configurations of f and g for parameters from sector B, when $\lambda, \mu < 1$. The coordinate x corresponds to ξ_L. Images adapted from [4].

In the remaining case that $\beta_1 > 0$ we have again that $\xi_L^f > \xi_L^g$ while $\beta_2 < 0$. Again, we find that f and g intersect for arbitrarily small values of β_1 and β_2, as seen in Figure 8(b). Thus, for parameter values in sector B there is a single limit cycle.

5.2 The second subcase $\lambda < 1$, $\mu > 1$

We now have $\lambda < 1$ and $\mu > 1$, which implies

$$\lim_{\xi_L \to 0} f(\xi_L) = \beta_2 \quad \text{and} \quad \lim_{\xi_L \to 0} f'(\xi_L) = \infty \tag{28}$$

while

$$\lim_{\xi_L \to \beta_1} g(\xi_L) = 0 \quad \text{and} \quad \lim_{\xi_L \to \beta_1} g'(\xi_L) = \infty \ , \tag{29}$$

so that now both f and g are convex upward. Note that $\lambda\mu < 1$ implies $\lambda < \frac{1}{\mu}$. For small values of the parameters, we may then expect the graph of f to be steeper than that of g.

We repeat the arguments from the first subcase, which now yield different results. Let us choose again a pair (β_1, β_2) of parameters from sector A. When $\beta_1 < 0$, we find that $f(0) > g(0)$ and $\beta_2 > 0$. Once more, this implies that there are no intersections between f and g, as seen in Figure 9(a).

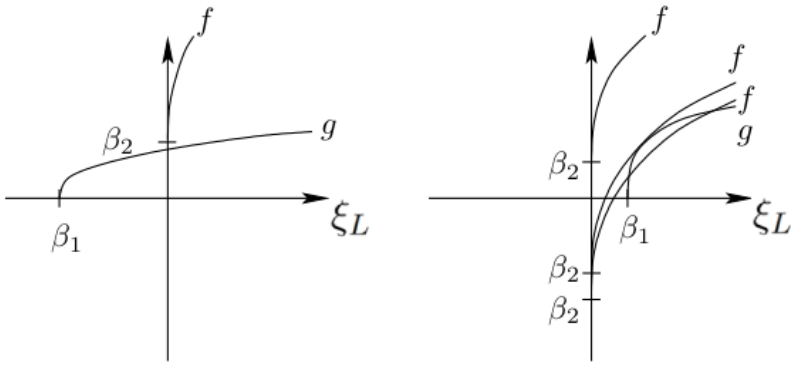

(a) $\beta_1 < 0$ (b) $\beta_1 > 0$

Figure 9: Possible configurations of f and g for parameters from sector A, when $\lambda < 1$ and $\mu > 1$. The coordinate x corresponds to ξ_L. Images adapted from [4].

When $\beta_1 > 0$, the situation changes. When $\beta_2 > 0$, there are still no intersections. However, when $\beta_2 < 0$, it must again hold that $\xi_L^f < \xi_L^g$, in which case there may now be none, one, or two intersections, and these possibilities are shown in Figure 9(b). We see that there exists one limit cycle if and only if f and g are tangent. This situation is structurally unstable, as the variation of parameters immediately results in either one or two limit cycles. We expect that there occurs a fold of cycles bifurcation.

Moving on to sector B, and assuming that $\beta_1 < 0$, we again obtain $f(0) < g(0)$ and $\beta_2 < 0$ or $\beta_2 > 0$. In this case, we find that there is one intersection of f and g, as seen in Figure 10(a).

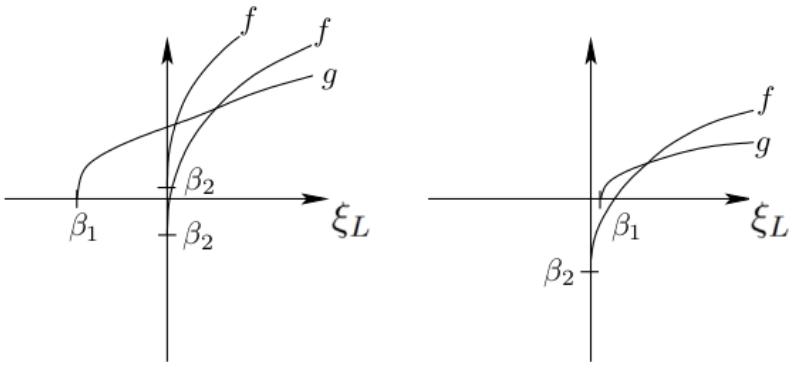

(a) $\beta_1 < 0$ (b) $\beta_1 > 0$

Figure 10: Possible configurations of f and g for parameters from sector B, when $\lambda < 1$ and $\mu > 1$. The coordinate x corresponds to ξ_L. Images adapted from [4].

The remaining case of $\beta_1 > 0$ implies that $\xi_L^f > \xi_L^g$, and that $\beta_2 < 0$, which together with the fact that f is steeper than g, as seen before, indicates that there is an intersection, visible in Figure 10. In conclusion, for parameters in sector B, there is again a single limit cycle.

5.3 Semi-stable cycle

The semi-stable cycle which appears at a fold of cycles bifurcation in the second subcase requires some extra analysis. As vector fields containing such a cycle are structurally unstable, it is necessary to know for which parameter values they appear when making the bifurcation diagram.

As seen in Section 5.2, the semi-stable limit cycle appears when f and g are tangent to each other. This means that $f(\xi_L) = g(\xi_L)$ and $f'(\xi_L) = g'(\xi_L)$, leading to

$$\beta_2 + \theta_1 \xi_L^\lambda = \left(\frac{\xi_L - \beta_1}{\theta_2} \right)^{\frac{1}{\mu}} \tag{30}$$

and

$$\lambda \theta_1 \xi_L^{\lambda-1} = \frac{1}{\mu \theta_2} \left(\frac{\xi_L - \beta_1}{\theta_2} \right)^{\frac{1}{\mu}-1} . \tag{31}$$

In [1], the following expression for β_2 in terms of β_1 is derived using the above two conditions,

$$\beta_2 = -\theta_2 \beta_1^\lambda - (1 - \mu^\mu) (\lambda \mu \theta_1 \theta_2)^{\frac{1}{1-\mu}} \beta_1^{\frac{\lambda-1}{1-\mu}} . \tag{32}$$

5.4 Heteroclinic connections

From the geometry of the monodromic case and the definition of the splitting parameters, it is clear that heteroclinic connections are only possible when one of the parameters is zero. Thus, in the bifurcation diagram, the curves corresponding to heteroclinic connections are the axes themselves.

5.5 Bifurcation Diagram Sketch

Taking into account the results for both subcases, we can now sketch their bifurcation diagrams. As stated previously, curves corresponding to homoclinic connections are denoted as P_L and P_M. In the second subcase, the curve in the parameter-plane corresponding to the semi-stable limit cycle is denoted by F. Curves corresponding to heteroclinic connections between saddles are denoted by the letter H and are labeled by the saddle from which they depart. Thus the curve corresponding to a heteroclinic connections from L to M is labeled with $H_{L,i}$, and vice versa, where $i = 1, 2$ is used to distinguish different scenarios. The value $i = 1$, related to the respective positive half axis of the parameter-plane,

indicates that the heteroclinic connections result from the unstable manifold of the other fixed point (M when the heteroclinic connection starts at L, and vice versa) in the heteroclinic contour of $\alpha = (0, 0)$ being broken outward. For $i = 2$, in the negative half axis of the parameter-plane, this now means that the unstable manifold of the other fixed point of the same heteroclinic contour is broken inward. The bifurcation diagram for the case where $\lambda, \mu < 1$ can be seen in Figure 11, and the one for the case where $\lambda < 1$ and $\mu > 1$ can be seen in Figure 12.

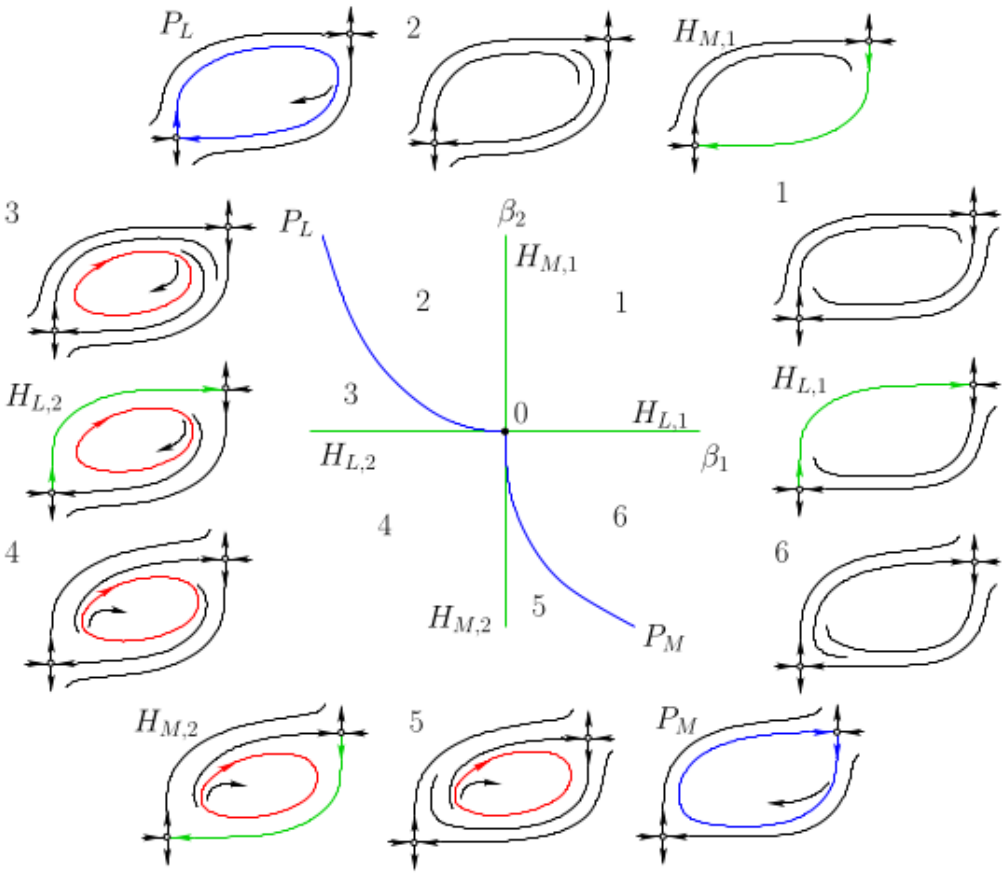

Figure 11: Bifurcation diagram of the monodromic heteroclinic contour for $\lambda, \mu < 1$. The blue curves correspond to homoclinic connections, while the green ones are heteroclinic connections. The red curves are limit cycles. For each relevant area of the parameter-plane and graphs we have a phase portrait showcasing the main features of the orbits. Image taken from [5].

Choosing initial parameter values on the curve P_L and varying the parameters through the bifurcation diagram in Figure 11 counterclockwise, we observe the following changes of the phase portrait in the first subcase. We begin on P_L with a homoclinic connection of the saddle L. This homoclinic connection is broken outwards and an unstable limit cycle is generated in accordance with the fact that $\lambda < 1$. Then, a heteroclinic connection from L to M is formed and destroyed when passing through the half axis $H_{L,2}$. In region 4 the unstable limit cycle persists, and then a heteroclinic connection from M to L is formed and destroyed when passing through the half axis $H_{M,2}$. On P_M, the unstable limit cycle disappears via a homoclinic connection of M , which then breaks inwards. This happens in accordance with $\mu < 1$. Under further variation of the parameters, a heteroclinic connection from L to M is formed and destroyed when passing through the half axis $H_{L,1}$, and a heteroclinic connection from M to L is formed and destroyed when passing through the half axis $H_{M,1}$. After region 2, we come back to curve P_L, where the original homoclinic connection of L is regained. In short, one might describe these changes as an interplay between two homoclinic bifurcations.

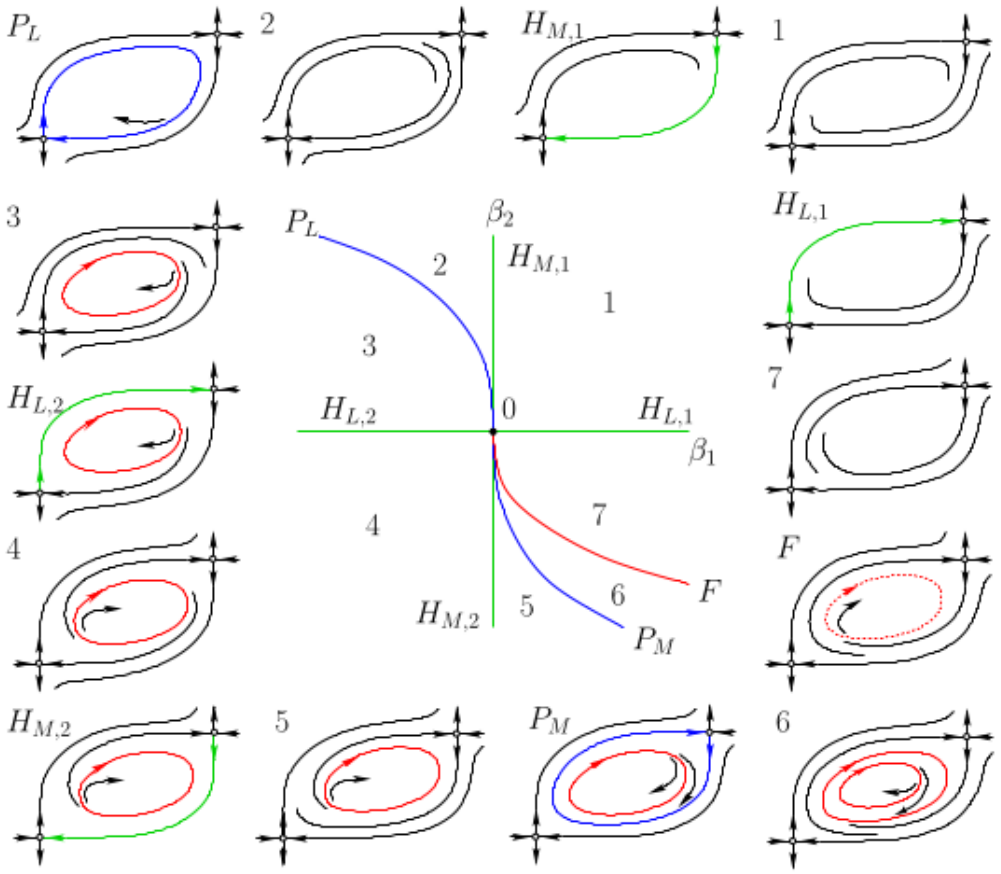

Figure 12: Bifurcation diagram of the monodromic heteroclinic contour for $\lambda < 1$ and $\mu > 1$. The blue curves correspond to homoclinic connections, while the green ones are heteroclinic connections. The red curves are limit cycles. For each relevant area of the parameter-plane and graphs we have a phase portrait showcasing the main features of the orbits. Image taken from [5].

In the second subcase, we perform the same analysis. Starting with certain parameter values and varying them counterclockwise through the bifurcation diagram in Figure 12. We begin on P_L with a homoclinic connection of L which is destroyed forming an unstable limit cycle. This behavior is not different from the first subcase, as it still holds that $\lambda < 1$. The evolution does not differ from the first subcase until a homoclinic connection of M is formed on P_M. In this process, the unstable limit cycle does not disappear, but now lies within the homoclinic connection. This happens in accordance with the fact that $\mu > 1$. Furthermore, when this connection is broken inwards, another limit cycle, now stable, is generated enclosing the original unstable one.

When reaching the curve F, these limit cycles collide, forming a single double limit cycle which is stable from the outside but unstable from the inside. This semi-stable and nonhyperbolic limit cycle is immediately destroyed, and under further variation of the parameters, a heteroclinic connection from L to M is formed and destroyed when passing through the half axis $H_{L,1}$, and a heteroclinic connection from M to L is formed and destroyed when passing through the half axis $H_{M,1}$. After region 2, we come back to curve P_L, where the original homoclinic connection of L is again formed. In short, one might describe these changes as the interplay between two homoclinic bifurcations resulting in a fold of cycles bifurcation.

6 A Monodromic Example

In this section we give an explicit two dimensional polynomial ODE exhibiting both possible types of bifurcations discussed in previous sections. The vector field

$$\begin{cases} \dot{x} = ax + by + cxy - ax^2 \\ \dot{y} = (a+b)y - (2a+2b+c)xy + 2cy^2 \end{cases} \tag{33}$$

has an invariant curve $\Gamma = G^{-1}(0)$, where $G(x,y) = y(y - x(1-x))$, for any values of a, b and c. This is the case beacuse in [5], this vector field is shown to be constructed from an algebraic variety with a shape similar to a monodromic heteroclinic contour. The variety corresponds to the union of a parabola described by $y = x(1-x)$ with the x-axis, leading to the $G(x,y)$ mentioned previously. It can be seen that this system has equilibria $L = (0,0)$ and $M = (1,0)$, however the types of these equilibria depend on the values of a, b and c. The Jacobian matrix of this vector field is given by

$$J(x,y) = \begin{pmatrix} a - 2ax + cy & b + cx \\ -(2a + 2b + c)y & (a+b) - (2a + 2b + c)x + 4cy \end{pmatrix} . \tag{34}$$

From this, we determine the eigenvalues at $(0,0)$ to be a and $a+b$, and the eigenvalues at $(1,0)$ to be $-a$ and $-a-b-c$. As a first example, we set $a = 1$, $b = -3$ and $c = 3/2$. We find that $\lambda_u = 1$ and $\lambda_s = -2$, so $\lambda = -\lambda_s/\lambda_u = 2 > 1$, while $\mu_u = 1/2$ and $\mu_s = -1$, making $\mu = 2 > 1$. With this, $\lambda\mu > 1$, implying that the heteroclinic contour is stable from the inside. We notice that these saddle indices correspond to subcase 5 in Table 1, treated in Section 5.1. A phase portrait of this system is given in Figure 13.

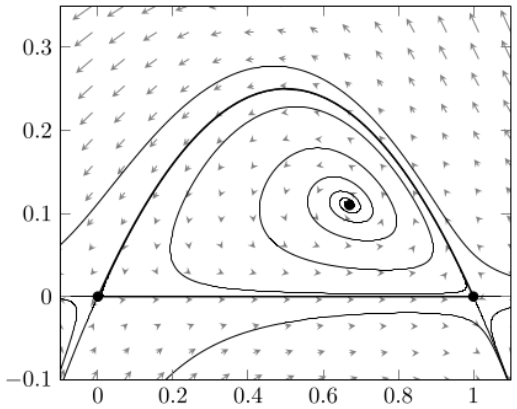

Figure 13: Phase portrait of system (33) for $a = 1$, $b = -3$ and $c = 3/2$. Image taken from [5]. Image taken from [5].

As a second example, we set $a = 1$, $b = -3$ and $c = 1/2$. This leads to $\lambda = 2 > 1$ but now $\mu_u = 3/2$ and $\mu_s = -1$, so $\mu = 2/3 < 1$ and $\lambda\mu = 4/3 > 1$, which corresponds to subcase 3 in Table 1. We recognize that we are in the situation of the second subcase treated in Section 5.2, after time reversal. A phase portrait of this system is shown in Figure 14.

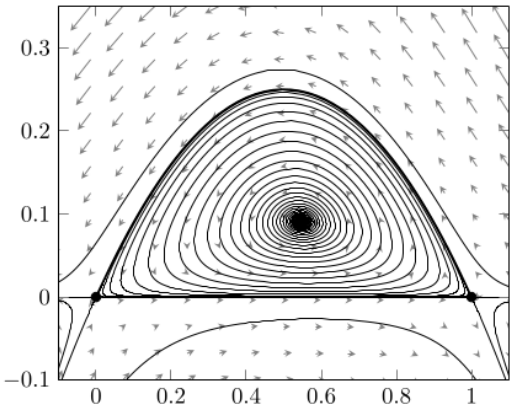

Figure 14: Phase portrait of system (33) for $a = 1$, $b = -3$ and $c = 1/2$. Image taken from [5].

In order to perform the bifurcation analysis we still need to add two parameter-dependent perturbing terms to system (33) which break the heteroclinic connections separately. As these connections can be described by the equations $y = x(1-x)$ and $y = 0$, this can be achieved by choosing parameters α and ε and adding the perturbing terms $\alpha(y - x(1-x))$ and εy to system (33). It is clear that the first perturbation does not affect the parabola while the second perturbation does not affect the straight line. We add one perturbing term to $\dot{x}$ and one to $\dot{y}$. This yields

$$\begin{cases} \dot{x} = ax + by + cxy - ax^2 + \varepsilon y \\ \dot{y} = (a+b)y - (2a+2b+c)xy + 2cy^2 + \alpha(y - x(1-x)) \ . \end{cases} \tag{35}$$

Now that we got the complete system, using the Matlab software package *MATCONT* allows for numerical bifurcation analysis of the equations (35) in both subcases. The numerical study of this polynomial system lets us compare the general diagram based on the behaviour of model maps, studied along Section 5, with an actual example of such a diagram. The analysis for the first case yields the bifurcation diagram in Figure 15, and the analysis in the second case leads to the diagram in Figure 17. To complete the study of these systems, representative phase portraits for parameter values in all components of the bifurcations diagrams are computed. They are displayed in Figures 16 and (18).

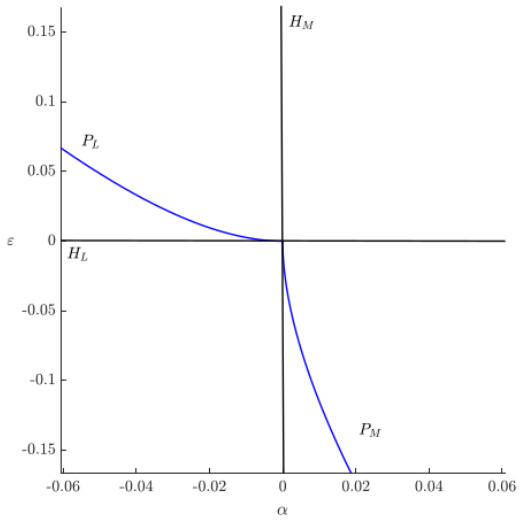

Figure 15: Parameter-plane diagram of the system (35) in the first subcase for $a = 1$, $b = -3$ and $c = 3/2$. Image taken from [5].

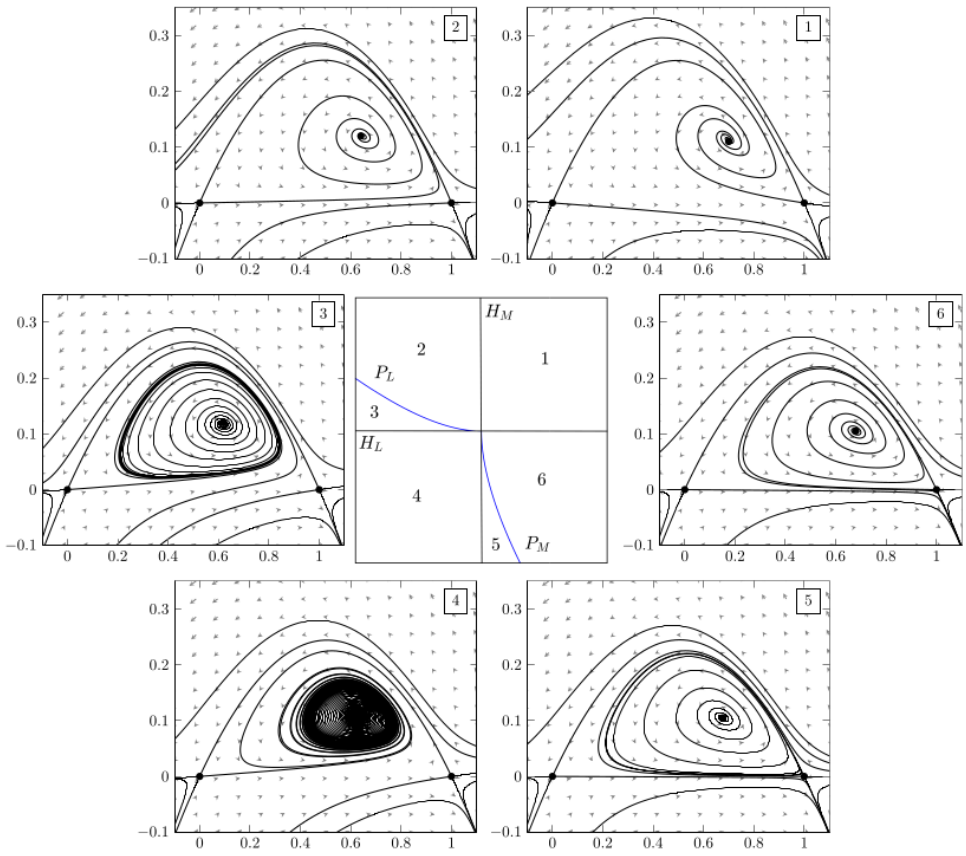

Figure 16: Full bifurcation diagram for the first subcase. Image taken from [5].

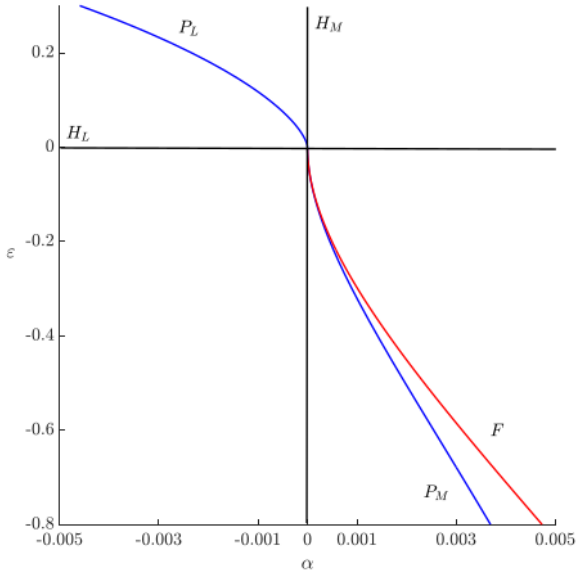

Figure 17: Parameter-plane diagram of the system (35) in the second subcase for $a = 1$, $b = -3$ and $c = 1/2$. Image taken from [5].

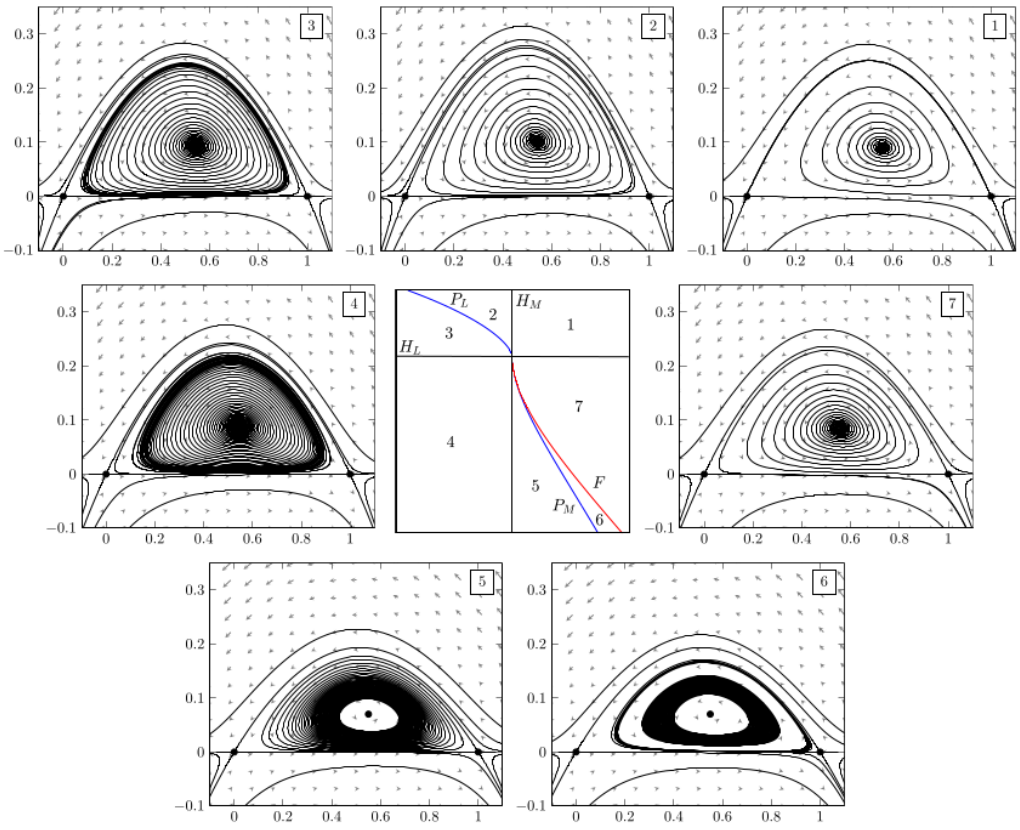

Figure 18: Full bifurcation diagram for the second subcase. Image taken from [5].

7 Conclusion

The theoretical results shown and discussed in this report are derived from the study of the truncated model maps. The work focuses on constructing the bifurcation diagrams that map transitions in the system phase portrait as parameters are varied for a monodromic heteroclinic contour. Two different subcases were investigated regarding the saddle indices of two equilibrium points, and from these two cases all the other possibilities can be deduced. Certain homoclinic and heterclinic connections were shown to be created and destroyed for $\lambda, \mu < 1$ and limit cycles appear in a specific part of the parameter plane as well. In general, the changes can be described as an interplay between two homoclinic bifurcations.

For $\lambda < 1$ and $\mu > 1$ a similar result was shown, but with the addition that the interplay between the two homoclinic bifurcations also results in a fold bifurcation, eventually leading to the emergence of a second stable limit cycle, enclosing the original unstable one. An explicit example of a two-parameter planar system with a monodromic heteroclinic contour was given, where the bifurcation analysis confirm all the theoretical work in the report.

References

[1] J. W. Reyn, *Generation of limit cycles from separatrix polygons in the phase plane*, p. 264–289. Springer Berlin Heidelberg, 1980.

[2] C. HSU, "Global analysis by cell mapping," *International Journal of Bifurcation and Chaos*, vol. 02, p. 727–771, Dec. 1992.

[3] A. V. Dukov, "Bifurcations of the 'heart' polycycle in generic 2-parameter families," *Transactions of the Moscow Mathematical Society*, vol. 79, p. 209–229, Nov. 2018.

[4] J. Hooyman, "Codim 2 bifurcations of planar heteroclinic contours."

[5] Y. A. Kuznetsov and J. Hooyman, "Bifurcations of heteroclinic contours in two-parameter planar systems: Overview and explicit examples," *International Journal of Bifurcation and Chaos*, vol. 31, p. 2130036, Sept. 2021.